Neuron, Vol. 37, 663–680, February 20, 2003, Copyright ©2003 by Cell Press

Orientation and Direction Selectivity of Synaptic Inputs in Visual Cortical Neurons: A Diversity of Combinations Produces Spike Tuning

Cyril Monier,[1] Frédéric Chavane,[1] Pierre Baudot, Lyle J. Graham,[2,*] and Yves Frégnac*
Unité de Neurosciences Intégratives et Computationnelles
CNRS-UPR 2191
91198 Cedex Gif-sur-Yvette
France

Summary

This intracellular study investigates synaptic mechanisms of orientation and direction selectivity in cat area 17. Visually evoked inhibition was analyzed in 88 cells by detecting spike suppression, hyperpolarization, and reduction of trial-to-trial variability of membrane potential. In 25 of these cells, inhibition visibility was enhanced by depolarization and spike inactivation and by direct measurement of synaptic conductances. We conclude that excitatory and inhibitory inputs share the tuning preference of spiking output in 60% of cases, whereas inhibition is tuned to a different orientation in 40% of cases. For this latter type of cells, conductance measurements showed that excitation shared either the preference of the spiking output or that of the inhibition. This diversity of input combinations may reflect inhomogeneities in functional intracortical connectivity regulated by correlation-based activity-dependent processes.

Introduction

Brain computation, in the early visual system, is often considered as a hierarchical process where features extracted in a given sensory relay are not present in previous stages of integration. In particular, many response properties in visual cortex, such as orientation and directional selectivities, are not present at the preceding geniculate stage, and a classical problem is identifying the mechanisms and circuitry underlying these computations. In order to assess how much synaptic integration of the network activity at each neuron contributes to the genesis of cortical orientation and direction selectivity, it is necessary to provide reliable measurements of the input/output transfer function at the single-cell level. In theory, a variety of combinations of excitatory and inhibitory input tuning can give rise to a given functional preference and tuning width in the spike response. Within this context, an important issue is whether cross-oriented or null-direction intracortical inhibition is fundamental for stimulus selectivity or rather only normalizes spike response tuning with respect to other features, such as stimulus strength or contrast. After a long-standing debate, most recent models favor the second possibility (see review in Ferster and Miller, 2000, and Douglas et al., 1999), largely because experimental support for the existence of inhibitory input in response to nonpreferred stimuli has been somewhat contradictory.

The essence of the feedforward model, initially proposed by Hubel and Wiesel (1962), was that Simple cortical cells inherit their orientation preference from the anatomical convergence of thalamic inputs. In order to reproduce contrast invariance of orientation tuning (Sclar and Freeman, 1982), this concept has been modified to include disynaptic intracortical inhibition acting in a so-called "push-pull" manner (Troyer et al., 1998). This model predicts that the modulation of both excitatory and inhibitory input is largest for the preferred stimulus. However, it is difficult to reconcile the apparent simplicity of feedforward schemas with the number and diversity of intracortical input sources impinging on cortical cells (Ahmed et al., 1994). Consequently, models of orientation tuning have been proposed that rely on recurrent excitatory connections to amplify the optimal component of broadly tuned and weak thalamic input (Douglas et al., 1995; Somers et al., 1995; Ben-Yishai et al., 1995). In this scheme, a typical postulate is that intracortical inhibition acts nonspecifically to maintain the selectivity of individual neurons by balancing intracortical excitation at the columnar level.

Nevertheless, a crucial role for inhibition has been indicated by pharmacological studies showing that $GABA_A$ antagonists can modify or eliminate both orientation and directional selectivity in cat primary visual cortex (Sillito, 1979; Sillito et al., 1980; Eysel and Shevelev, 1994), although attempts to block $GABA_A$ receptors intracellularly appeared not to change the qualitative orientation preference of the cell (Nelson et al., 1994). In addition, disinhibition experiments give strong evidence for an inhibitory shaping of orientation and direction selectivity by neighboring or distant columns (Eysel et al., 1990; Crook et al., 1997). Furthermore, these disinhibitory effects seem to be correlated with the anatomy of the intracortical inhibitory network (Crook et al., 1998; Roerig and Kao, 1999; Buzas et al., 2001). Some models of orientation and direction selectivity, incorporating nonspecific or nonoptimal inhibition, account partially for these different experimental results (Ferster and Koch, 1987; Wörgötter and Koch, 1991; Adorjan et al., 1999; McLaughlin et al., 2000; Ruff et al., 1987; Sabatini and Solari, 1999). However, currently available electrophysiological evidence supporting these models remains controversial. While intracellular recordings rather consistently show the presence of inhibition in response to the preferred orientation, as well as in some cases the direction opposite to the preferred one, no firm agreement has yet been reached concerning its presence for orientations outside the spike tuning range. Early intracellular recordings (Benevento et al., 1972; Creutzfeldt et al., 1974; Innocenti and Fiore, 1974) showed

*Correspondence: yves.fregnac@iaf.cnrs-gif.fr (Y.F.), lyle@biomedicale.univ-paris5.fr (L.J.G.)
[1]These authors contributed equally to this work.
[2]Present address: UMR 8119 CNRS, Université René Descartes, Neurophysique et Physiologie du Systèm Moteur, UFR Biomédicale, 45 rue des Saint-Peres, 75270 Paris Cedex 06, France.

strong hyperpolarizations in response to stimuli in the null direction and, occasionally, to cross-orientated stimuli. Later studies confirmed that prominent hyperpolarizations could be evoked by stimuli with nonoptimal orientations (Volgushev et al., 1993), depending of the laminar location of the cell (Martinez et al., 2002). However, other studies failed to reproduce these qualitative findings, reporting only iso-oriented hyperpolarizations (Ferster, 1986) or occasional hyperpolarizations for nonoptimal orientations in some complex cells (Douglas et al., 1991).

Detecting inhibitory input on the basis of evoked changes in membrane potential may prove to be difficult, since the reversal potential of $GABA_A$-controlled chloride channels is situated near the resting membrane potential of cortical neurons. This shunting inhibition may reduce the effect of concomitant excitation by evoking a large increase in input conductance while leaving the membrane potential relatively unaffected. Two strategies can be used to unmask this "silent" inhibition: the first one is to depolarize the cell in current clamp sufficiently to change the balance in the driving forces for inhibition versus excitation. Using this method, Ferster (1986) reported that hyperpolarizing potentials recorded in the depolarized state had the same selectivity for orientation as depolarizing potentials.

The second approach is to estimate conductance changes during visual stimulation. First attempts using sample-based methods did not succeed in showing changes of synaptic conductance whether the applied stimulus feature was a preferred or a nonpreferred one (Douglas et al., 1988; Berman et al., 1991; Ferster and Jagadeesh, 1992; but see Bush and Sejnowski, 1994). In spite of these negative reports, we previously applied an in vivo whole-cell voltage-clamping method to continuously track both the evoked conductance and the apparent synaptic reversal potential during visual responses of neurons in primary visual cortex. We demonstrated large transient shunting inhibition conductance increases for optimally oriented flashed stimuli (Borg-Graham et al., 1996, 1998). Using a similar method, but in current-clamp mode, a growing number of experimenters have since confirmed the presence of shunting inhibition in vivo (Hirsch et al., 1998; Anderson et al., 2000b). Furthermore, Anderson et al. (2000b) reported that, for any given cell, the excitatory and inhibitory conductances had similar preferred orientations and tuning widths, highly correlated with that expressed by the firing tuning curve, whatever the laminar location of the postsynaptic cell.

Faced with the diversity of the experimental observations concerning the presence or absence of inhibitory input evoked by nonpreferred orientation or directions, we have re-addressed this issue with a quantitative comparative study combining several of the electrophysiological protocols mentioned above. Both sharp and patch electrodes were used in order to take advantage of complementary benefits provided by each technique applied in the same in vivo preparation.

Results

The approach we present here is to revisit, step-by-step, intracellular evidence for the presence of inhibitory input in nonpreferred orientations/directions and to determine how the tunings of the excitatory and inhibitory inputs are related to that of the spiking output. Where possible, several complementary approaches were compared and combined in the same cell in order to compensate the limitations inherent to each method.

One set of protocols was based on passive measurement of intracellular potentials under current clamp. As a first step, at the resting membrane potential, we measured the tunings of evoked increases and decreases in spiking rate. We then measured the tunings of the depolarizing and hyperpolarizing components of the subthreshold synaptic activity. We also measured the inverse of the trial-to-trial variability ($1/\sigma$) of the stimulus-locked membrane potential waveform. Our hypothesis was that an increase in input conductance might produce a reduction in the trial-to-trial variability of the membrane potential trajectory independently of any change in the mean. Thus, an increase in $1/\sigma$ could signal the presence of shunting inhibition.

Since the presence of hyperpolarization can be masked by concurrent excitation, especially in the preferred orientation or direction, another set of protocols was aimed at increasing the visibility of synaptic input and allowing the quantitative measurement of this input. First, the inhibitory drive was amplified and the excitatory drive reduced by depolarizing the postsynaptic membrane potential in current clamp sufficiently to fully inactivate spike-related currents. This method reveals visually evoked inhibition as hyperpolarizations. In the second approach, limited to low-access resistance patch recordings, we measured the continuous dynamics of the total synaptic conductance input and the associated reversal potential during the visual stimulation. Decomposition methods were then applied to dissect out the respective tuning of excitatory and inhibitory conductances (see Experimental Procedures).

Orientation and direction tuning curves were measured using moving bars whose direction of motion was perpendicular to orientation and which were swept across the full extent of the subthreshold visual receptive field (Bringuier et al., 1999). To facilitate comparison between the various response components presented above, we used the same quantifications in all cases, based on the integral calculated over the entire duration of visual stimulation. Statistical significance was tested against the nonstimulated condition. The optimal direction (OD), the tuning width (HWHH), and the nonorientation selective part ("Base") of each response component were estimated by fitting the response integral as a function of stimulus direction by two Gaussians forced to peak 180° apart. Importantly, the fit for each component was made independently of the other (see Discussion). Each response component was then classified into one of four categories depending on the comparison between its optimal direction and the preferred direction expressed by the spike response: "Iso-P" for angular difference ranging between 0° to 30°; "Oblique" for differences between 30° to 60° or 120° to 150°; "Cross" for differences between 60° to 120°; and "Iso-N" for differences between 150° to 180°.

The present study is based on the quantitative analysis of 88 cells recorded using sharp ($n = 39$) and whole-cell patch ($n = 49$) electrodes, for which the receptive

field (RF) was characterized by sparse noise mapping (51 simple [25 S1 and 26 S2-S3], 32 complex, and 5 unclassified), and the orientation selectivity of subthreshold and spiking activity was measured in response to moving bars. The spontaneous activity and the peak firing rates for the preferred stimulus were higher for sharp than for patch recordings (spontaneous activity: 3.8 ± 5 a.p./s (n = 39) versus 0.3 ± 0.5 a.p./s (n = 49), $p < 0.01$; and peak firing rate: 52 ± 28 a.p./s (n = 39) versus 32 ± 27 a.p./s (n = 49), $p < 0.01$). In about one quarter (20/88, 23%) of the cells, a clearly bimodal or two-state distribution of the spontaneous membrane potential was apparent in both patch and sharp recordings (see also Anderson et al., 2000a).

Spike and Depolarizing Responses

All cells presented a significant depolarizing response in at least one direction, with a mean peak depolarization amplitude for the optimal stimulus in the order of 10mV (9.5mV ± 4.8mV, n = 88). The orientation tuning of depolarizing responses was, on average, significantly wider than that of spiking responses (HWHH: 46° ± 13° vers 30° ± 9°, Base: 23% ± 19% versus 5.6% ± 8%, $p < 0.01$, n = 88). However, the improvement in orientation selectivity between the depolarizing and the spiking responses (mean of the difference in tuning width: 15° ± 13°, n = 88) was highly variable between cells (range for the difference: −10° to 60°, see example in Figures 1, 3, and 4). As expected, the optimal direction derived from the subthreshold depolarizing response tuning and that expressed in the spike discharge tuning was similar for a large majority of cells [82% of Iso-P cases, shown in the red histogram (Dep.) of the left column in Figure 2]. Nevertheless, some cases were observed where the largest depolarization (measured by its integral value) was obtained for nonpreferred orientations (11%) or null-directions (7%).

Suppression of Spike Discharge and Hyperpolarizing Responses

In one quarter of the cells (23/88, 26%) for which background activity was high enough to detect periods of significant spike rate decrease, it was possible to establish the range of orientations or directions for which a suppression of background activity (integrated only over the periods where it is detected during the whole stimulus exploration) was induced by the visual stimulus (shaded tuning curves in left column, for cell 1 in Figure 1 and cell 6 in Figure 3). The overall distribution of the optimal direction derived from the spike suppression component shows dominance for cross-orientation preference (Cross: 11/23, 48%) and null direction (Iso-N: 6/23, 26%). The tuning width of the suppression was generally broader than that of the spike (HWHH: 48.1° ± 20°; base: 15% ± 12%, n = 23).

Significant hyperpolarizing responses from rest could be detected for at least one direction in half of the cells (42/88, 48%). The mean peak amplitude (calculated over a 25 ms period) of the hyperpolarization component was 3.7mV ± 1.8mV (n = 42). The probability of detecting evoked hyperpolarizations appeared to depend on the initial resting potential, since the average resting potential of cells with significant hyperpolarizing responses was more depolarized than that of the remaining cells (−64mV ± 4mV (n = 42) versus −69mV ± 6mV (n = 46), $p < 0,01$). The hyperpolarizing component had a tuning width of 40° ± 16° with a base component equal to 11% ± 12% of the peak amplitude. The summary distribution ("Hyp." in Figure 2) shows that the direction preference of the hyperpolarizing component differs from that expressed by the spike response. Almost two-thirds of the cells showed the optimal hyperpolarizing response for either cross-oriented (Cross: 18/42, 43%, see Figure 1, cells 1 and 2) or oblique directions (Oblique: 9/42, 21%, see Figure 3, cell 6). The remaining third of the cells had dominant hyperpolarizing responses for either the preferred direction (Iso-P: 9/42, 21%, see Figure 1, cell 3) or for the null direction (Iso-N: 6/42, 14%, see Figure 4, cell 11). Of the 23 cells with significant background spike activity, 14 showed both significant spike suppression and hyperpolarizing responses, with similar optimal direction preference ($r^2 = 0.77$, $p < 0.01$, n = 14). Cells with a cross-oriented optimal hyperpolarizing component were significantly less direction selective than cells with an iso-oriented optimal hyperpolarizing component (DI: 0.48 ± 0.27 [n = 18] versus 0.75 ± 0.24 [n = 15], $p < 0.01$).

Trial-to-Trial Variability of the Membrane Potential

It was expected that the presence of a shunting inhibition might cause a significant reduction of trial-to-trial variability in the trajectory of the membrane potential independently of any significant hyperpolarization or depolarization during the visual response. We therefore calculated the inverse of the standard deviation of the membrane potential waveform synchronized with the stimulus onset (see Vm ± S.D. and $1/\sigma$, green trace in cell 2 in Figure 1) and compared this with the baseline level observed in the absence of visual stimuli.

A majority of cells (52/88, 59%) showed a significant reduction of trial-to-trial variability during visual stimulation in at least one direction. The mean peak amplitude of the $1/\sigma$ component was 183% ± 67% (n = 52) and was observed at similar membrane potential values in different cells (−66.4mV ± 4.4mV [n = 52]). These cells exhibited a significantly higher trial-to-trial variability in their pre-trigger spontaneous membrane potential activity than the rest of the population (i.e., for $1/\sigma$: $0.3mV^{-1}$ ± $0.1mV^{-1}$ [n = 52] versus $0.8mV^{-1}$ ± $0.7mV^{-1}$ [n = 36], $p < 0.01$), suggesting that a certain fluctuation level in the synaptic background activity has to be present in order to detect a significant reduction in evoked variability.

About half (24/52, 46%) of the cells that showed a significant reduction in trial-to-trial variability also showed significant evoked hyperpolarizations (see cells 2 and 3, Figure 1), and the orientation preferences of the two components were found to be correlated ($r^2 = 0.70$; $p < 0.01$ [n = 24]). In spite of this similarity and as summarized in the left column in Figure 2 (see Hyp and $1/\sigma$ rows), the tuning width of the $1/\sigma$ component was, on average, larger than that of the hyperpolarizing component (HWHH: 50° ± 18° versus 41° ± 19°, $p < 0.05$ [n = 24]). For the majority of these cells, the largest reduction of variability was evoked for nonpreferred directions or orientations (Cross and Oblique: 20/24, 83%).

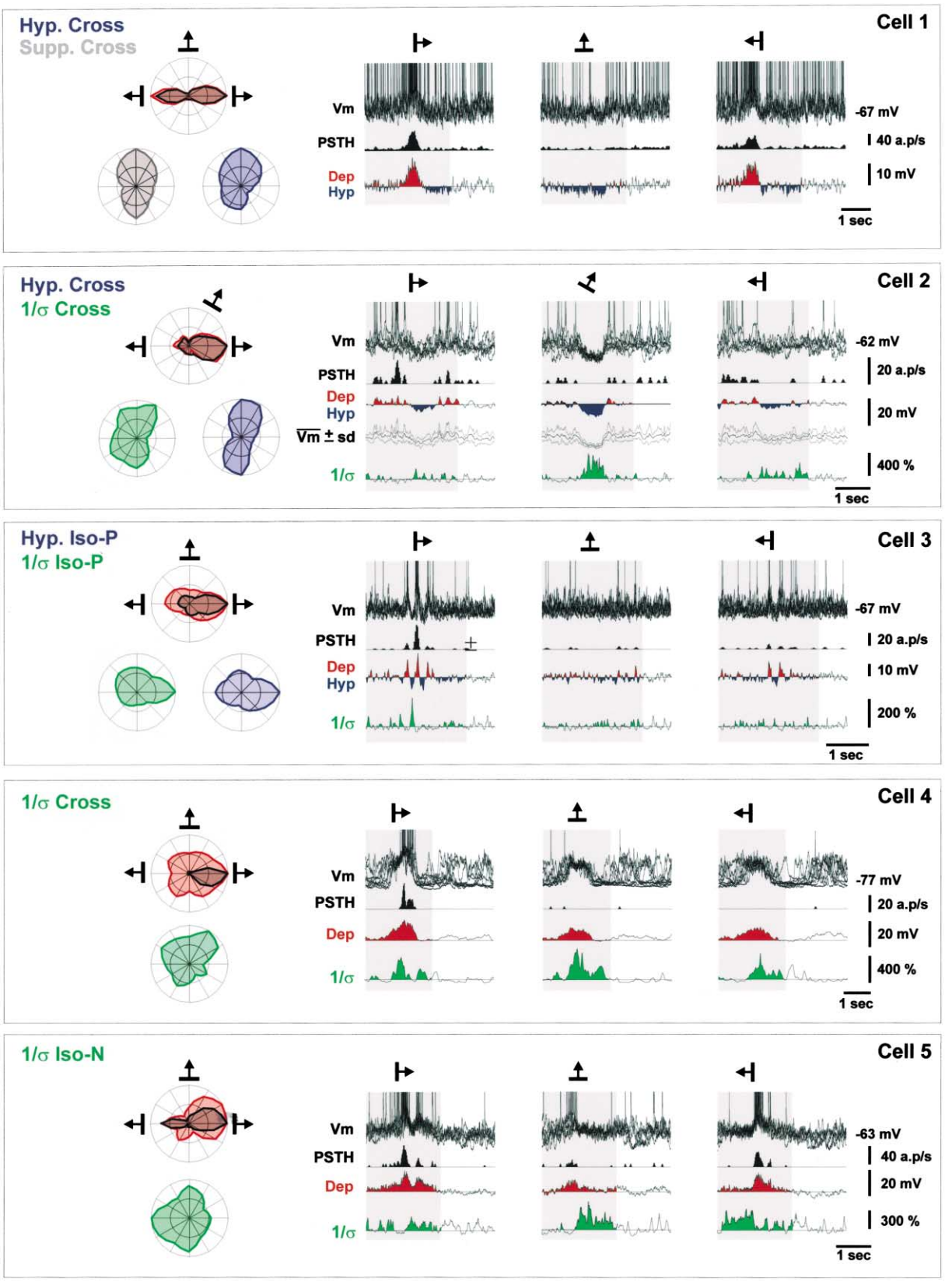

Figure 1. Measurements of Visual Activity, Evoked from the Resting State

This figure shows five examples of whole-cell patch and sharp recordings, each row illustrating one cell. Each inset shows, from top to bottom, the time course of evoked responses obtained at rest for the membrane potential (five to ten superimposed trials, truncated spikes), for spike

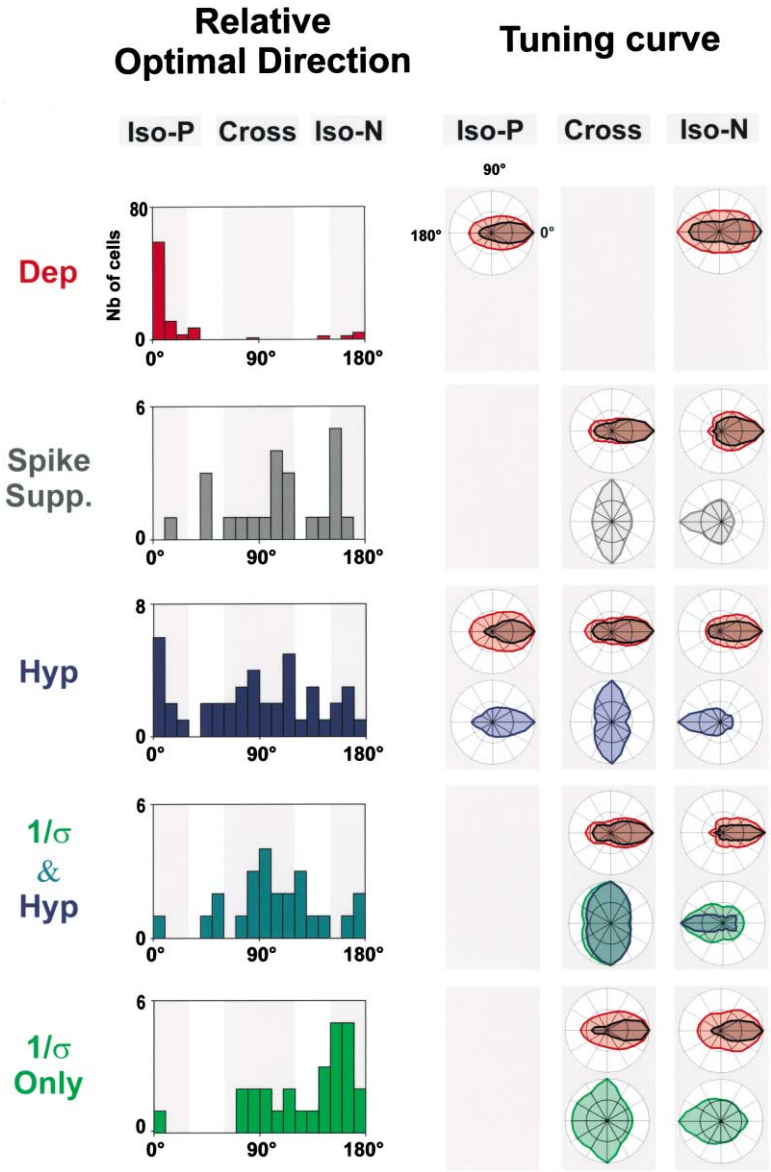

Figure 2. Measurements of Visual Activity, Evoked from the Resting State: Population Analysis

The left column presents, for each component, the distribution of the optimal direction (OD) relative to the spike preferred (set to 0°): spike suppression (Spike Supp.), depolarization (Dep), hyperpolarization (Hyp), inverse of trial-to-trial variability concomitant with a significant hyperpolarization ($1/\sigma$ and Hyp) and without significant hyperpolarization ($1/\sigma$ only). The right panel presents the averaged tuning curves of the various components for different subpopulations of cells defined on the basis of their optimal direction relative to the preferred direction: Iso-P, Cross-, or Iso-N. Cells with a component that had an oblique preference are not included in the averaged polar plots.

We also recorded from cells in which a reduction in trial-to-trial variability during the visual response was seen without changes in membrane potential or with a concomitant depolarization of the mean membrane potential (Figure 1, cells 4 and 5). For these cells (28/52, 54%), the tuning width of the variability reduction effect was broad (HWHH: 61° ± 19°, n = 28), and the distribution of the direction preference derived from the $1/\sigma$ tuning curve (Figure 2, $1/\sigma$ only) showed a strong peak for the null-direction. For the cells that showed a two-state behavior (15/28, 54%), visual stimuli tended to clamp the membrane potential in the up-state independently of the stimulus direction, resulting in a significant reduction in trial-to-trial variability associated with a strong depolarization. However, the strength of this variability-reducing effect still depended on stimulus orientation (compare the up-state variability observed for the cross- and the null-directions in cell 4 of Figure 1).

counts (black, PSTH) and for subthreshold activity (depolarization in red [*Dep*]; hyperpolarization in blue [*Hyp*]) for three particular stimulus directions (left, preferred direction [0°]; middle, cross-orientation [60°–120°, 240°–300°]; right, null-direction [180°]). The left column presents polar plots of the different response components with their respective color codes. To facilitate comparisons in the polar plots of this and the subsequent figures, the direction eliciting the best spiking response was set to 0° for all cells, pointing to the right. For direct comparison, the tunings of the spike and depolarizing responses are overlaid on the same plot. Cross-oriented hyperpolarization and spike suppression are illustrated in cell 1 (Sharp, Simple RF; optimal directions [OD]: Dep. 1°, Supp. 88°, and Hyp. 81°). Concomitant hyperpolarization and $1/\sigma$ components are illustrated in cell 2 (Patch, Complex RF; OD: *Dep* 0°, *Hyp* 80°, and *1/σ* 90°) and cell 3 (Sharp, Simple RF; OD: *Dep* 5°, *Hyp* 0°, *1/σ* 6°). Reduction of trial-to-trial variability associated with depolarizing or null mean response is illustrated in cell 4, which had a bistable behavior (Patch, Complex RF; OD: *Dep* 9° and *1/σ* 79°), and cell 5 (Patch, Simple RF; OD: *Dep* 5° and *1/σ* 152°).

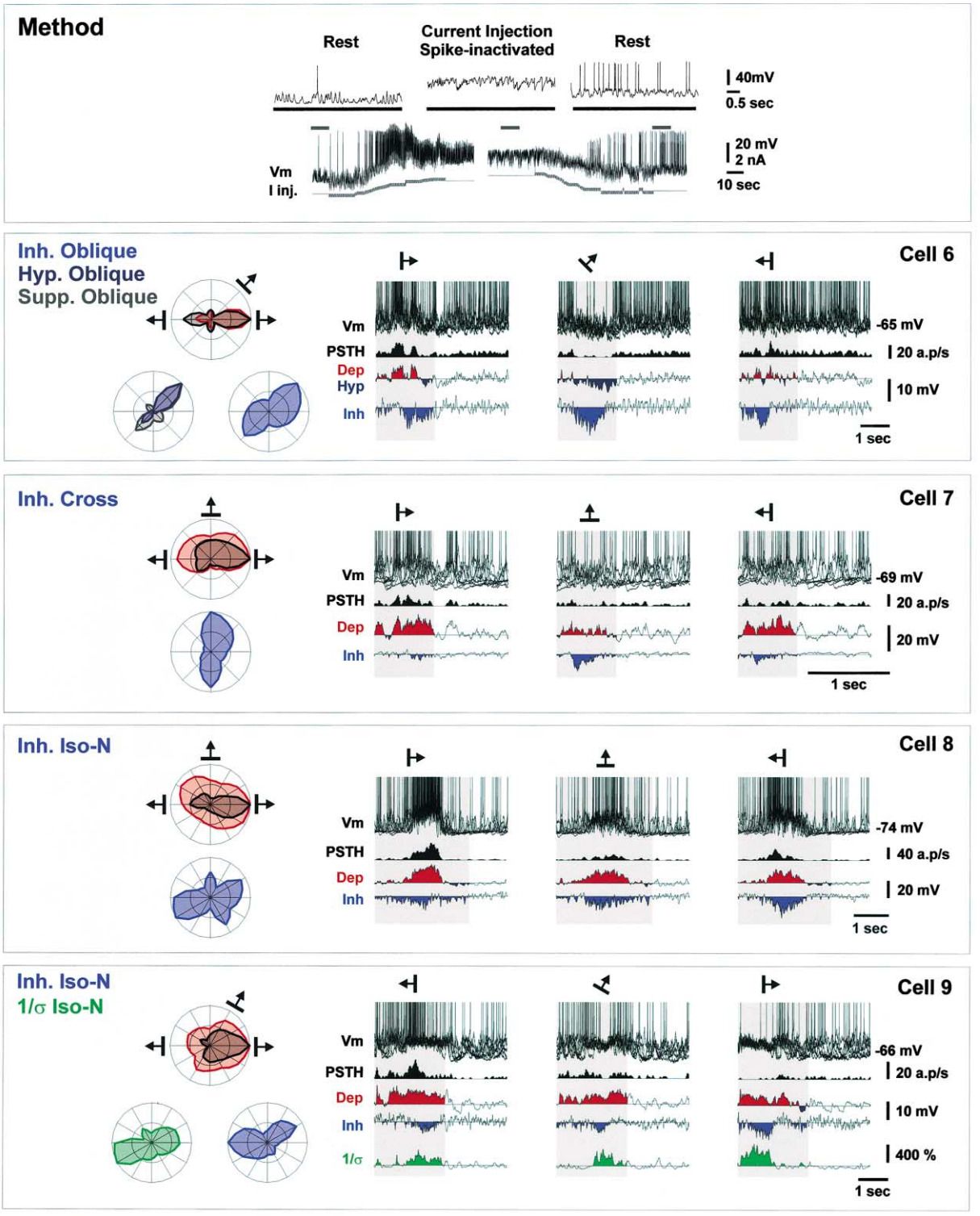

Figure 3. Inhibition Revealed by Spike-Inactivated Protocols

This figure presents four examples of sharp recordings for which a reversible spike-inactivated protocol was applied, each panel illustrating one cell. The method is summarized in the top inset. A depolarizing current was injected, and its intensity level was adjusted to inactivate spike initiation. The presence of IPSPs can be seen as hyperpolarizations in the membrane potential during current injection. The end of the trace illustrates the reversibility of the protocol. Inhibitory (Inh), hyperpolarization, and spike suppression components with an oblique preference are illustrated in cell 6 (Sharp, Simple RF; OD: Dep. 3°, Supp. 46°, Hyp. 46°, and Inh. 41°). Cross-oriented inhibitory components are illustrated in cell 7 (Patch, Complex RF; OD: *Dep* 2° and *Inh* 118°). Cell 8 illustrates the case of an inhibitory component in the Null direction (Sharp, Complex RF; OD: *Dep* 12° and *Inh* 161°). A similar finding was observed for cell 9, for which both the time course and orientation tuning of the inhibitory and *1/σ* components were highly correlated (Sharp, complex RF; OD: *Dep* 7°, *1/σ* 159°, and *Inh* 177°).

Unmasked Inhibition by Spike-Inactivated Protocols

The results presented above suggest the presence of inhibitory input for both preferred and nonpreferred orientations. However, inhibition evoked by the preferred stimulus (i.e., that eliciting the strongest spike discharge) may be underestimated, since it could be masked when concomitant excitation dominates and the cell fires. To address this possibility, as well as to improve the visibility of inhibitory inputs as hyperpolarizing events, we increased the inhibitory driving force by depolarizing the cell (Figure 3, see method panel) using intracellular current injection sufficient to inactivate fast Na channels and thus completely suppress spike activity. In this spike-inactivated state, only hyperpolarizing responses were significant, giving a reliable indication that the holding potential was close to the reversal potential of excitatory input. This protocol was applied successfully and reversibly in nine cells, for which we could compare the tuning curves of the evoked hyperpolarizing responses observed in the spike-inactivated state (Inh, inhibitory component; Figure 3), with the spike tuning curves established at rest (without current injection).

Figure 3 illustrates five cells in which visually evoked spike and subthreshold responses were compared with the inhibitory response component. The main result is the striking diversity of the distribution of inhibitory input observed in different cells: one third of cells (3/9) had an inhibitory component with an optimal direction in the preferred direction, one third in the oblique- (1/9, see cell 6, Figure 3) or cross- (2/9, see cell 7, Figure 3) orientation preference, and one third (3/9) in the null-direction (see cells 8 and 9, Figure 3). The HWHH of the tuning curves of the inhibitory component measured in the spike-inactivated state was on average of $43° \pm 16°$ ($n = 9$) with a base of $29\% \pm 18\%$. The diversity in the respective tuning preferences of spike output and the inhibitory input revealed in the spike-inactivated state is further summarized in Figures 5 and 6.

The hyperpolarizations evoked in the spike-inactivated state were larger in amplitude and duration than those seen at the resting state, when this latter component was detectable. For cell 6 in Figure 3, the amplified evoked hyperpolarizations exhibited the same oblique preference as the hyperpolarizations at rest and the suppression of the spike component but with a wider tuning due to the unmasking of inhibition for both the preferred and null directions. Cells 7, 8, and 9 (Figure 3) showed only depolarizing components under the control condition, whereas the presence of an inhibitory component was revealed in all directions under depolarizing current, with either a cross-oriented (cell 7) or null-direction preference (cells 8 and 9). The time course of the inhibitory component waveform reproduced precisely that observed for the reduction in membrane potential trial-to-trial variability at rest, giving further evidence that the decrease of variability indeed reflects a dominant inhibitory input. The two cases where the orientation preference of the hyperpolarizing components was not the same at rest and in the spike-inactivated state corresponded to a shift from cross- to iso-preference, and from oblique- to cross-preference, suggesting no systematic bias in the revealed component relative to the spike-based preference.

Excitatory and Inhibitory Conductances

The results obtained so far show that the tuning of inhibitory input can be unmasked and qualitatively studied in the spike-inactivated state. However, these experiments do not provide a direct quantitative estimate of the excitatory and inhibitory tunings. The continuous measure of input conductance and the apparent reversal potential during the visual response advances one step closer toward the identification of the orientation or direction dependence of synaptic inputs (Borg-Graham et al., 1998; Borg-Graham, 2001). Voltage-clamp measurements of excitatory and inhibitory conductances and their orientation or direction tuning were successfully achieved with low access resistance for 12 cells (see example of VC recordings in cell 13, Figure 4). We also estimated conductance components in current-clamp mode in seven cells. Since similar results were obtained with both methods when tested on the same cells ($n = 3$), data were pooled for further population analysis (16 cells and 19 protocols in total).

The relative increase in global peak conductance was similar, on average, for different populations of cells when evoked by moving stimuli or by flashed stimuli ($110\% \pm 60\%$ [$n = 19$] versus $113\% \pm 58\%$ [$n = 7$] [Borg-Graham et al., 1998]), and the range (35% to 270%) was equally variable among cells. The relative contribution of excitation and inhibition in the input tuning was examined using a three-term decomposition algorithm to extract one excitatory (AMPA) and two inhibitory synaptic components ($GABA_A$ and $GABA_B$) of the evoked conductance change. Note that the possible nonlinear implication of NMDA receptor activation was not taken into account by the decomposition model. Results show that in most cases the influence of the $GABA_B$ component was minor. The several examples shown in Figure 4, which illustrate only the AMPA and $GABA_A$ components of the conductance change, show a large diversity of tuning combinations for excitatory and inhibitory conductance increases.

Establishing the relative strength of conductances by integrating synaptic input for each stimulus direction may give only a partial understanding of the effectiveness of the interaction between excitation and inhibition. An additional key feature in the genesis of functional preference is the temporal overlap of both types of inputs, which act out of phase or in-phase. To explore these temporal relationships, the waveforms of the excitatory and inhibitory conductances were cross-correlated for each direction of the stimulus, and a normalized correlation index at zero-time lag was used to quantify their temporal overlap (TO: 0% for anti-phase, 100% for in-phase, see Experimental Procedures).

Over the whole population, only three major types of interaction between excitatory and inhibitory tuning were found for both orientation and direction selectivity on the basis of their similarity ("Preferred" [P]) or dissimilarity ("Non-Preferred" [NP]) to the spike output preference, distinguishing between (1) those cells in which excitatory and inhibitory input were tuned for the preferred direction or orientation (P-P); (2) those where the excitatory input was tuned for the preferred stimulus, but the inhibition was tuned for the nonpreferred stimulus (P-NP); and finally, (3) those where excitatory and inhibitory inputs were tuned for the nonpreferred stimu-

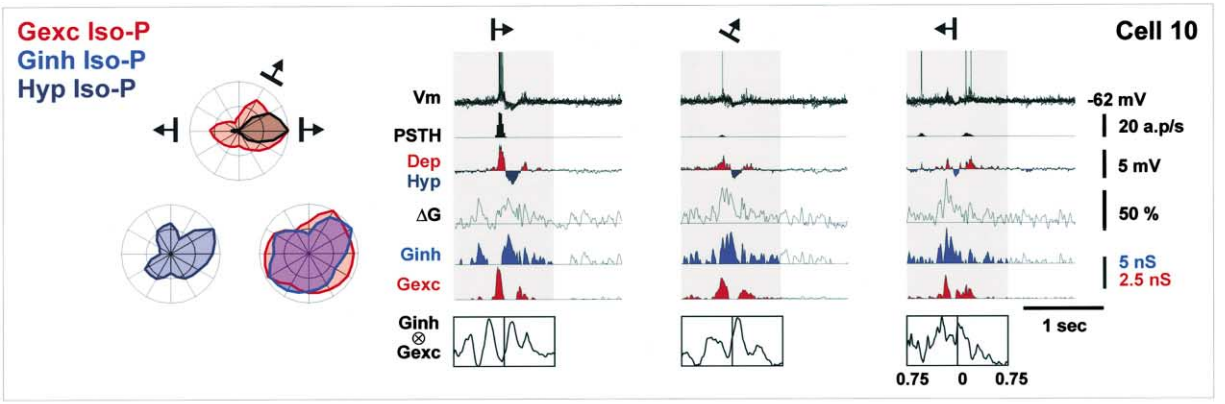
Gexc Iso-P
Ginh Iso-P
Hyp Iso-P
Cell 10
Vm
PSTH
Dep
Hyp
ΔG
Ginh
Gexc
Ginh
⊗
Gexc
-62 mV
20 a.p/s
5 mV
50 %
5 nS
2.5 nS
1 sec
0.75 0 0.75

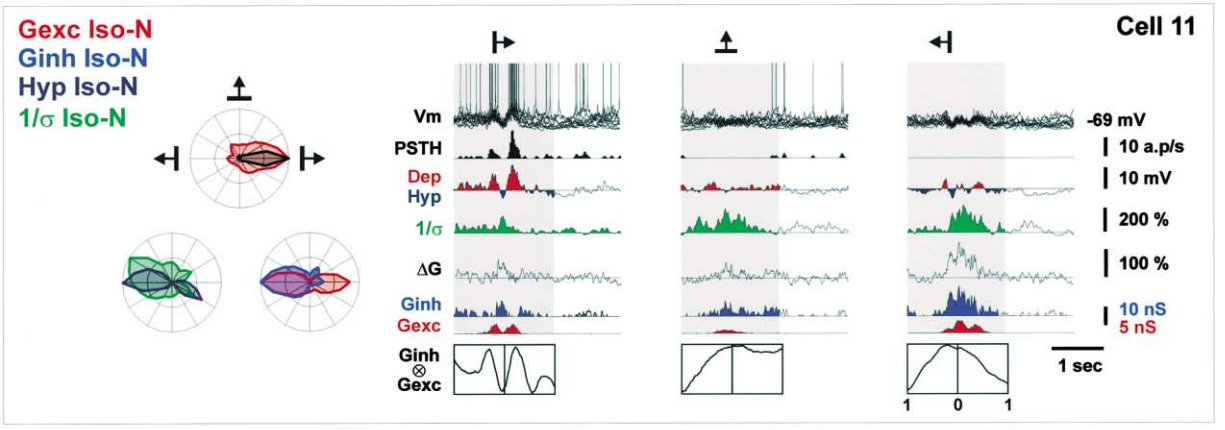
Gexc Iso-N
Ginh Iso-N
Hyp Iso-N
1/σ Iso-N
Cell 11
Vm
PSTH
Dep
Hyp
1/σ
ΔG
Ginh
Gexc
Ginh
⊗
Gexc
-69 mV
10 a.p/s
10 mV
200 %
100 %
10 nS
5 nS
1 sec
1 0 1

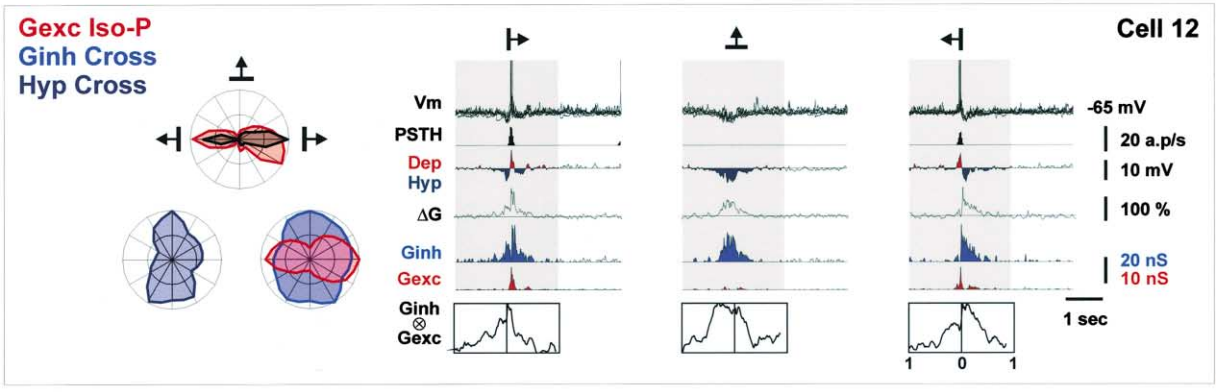
Gexc Iso-P
Ginh Cross
Hyp Cross
Cell 12
Vm
PSTH
Dep
Hyp
ΔG
Ginh
Gexc
Ginh
⊗
Gexc
-65 mV
20 a.p/s
10 mV
100 %
20 nS
10 nS
1 sec
1 0 1

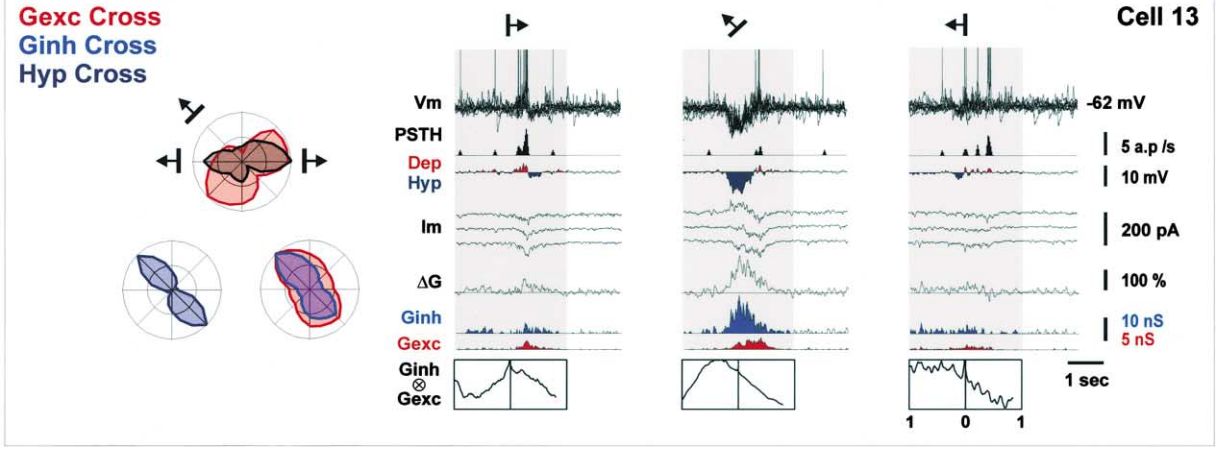
Gexc Cross
Ginh Cross
Hyp Cross
Cell 13
Vm
PSTH
Dep
Hyp
Im
ΔG
Ginh
Gexc
Ginh
⊗
Gexc
-62 mV
5 a.p /s
10 mV
200 pA
100 %
10 nS
5 nS
1 sec
1 0 1

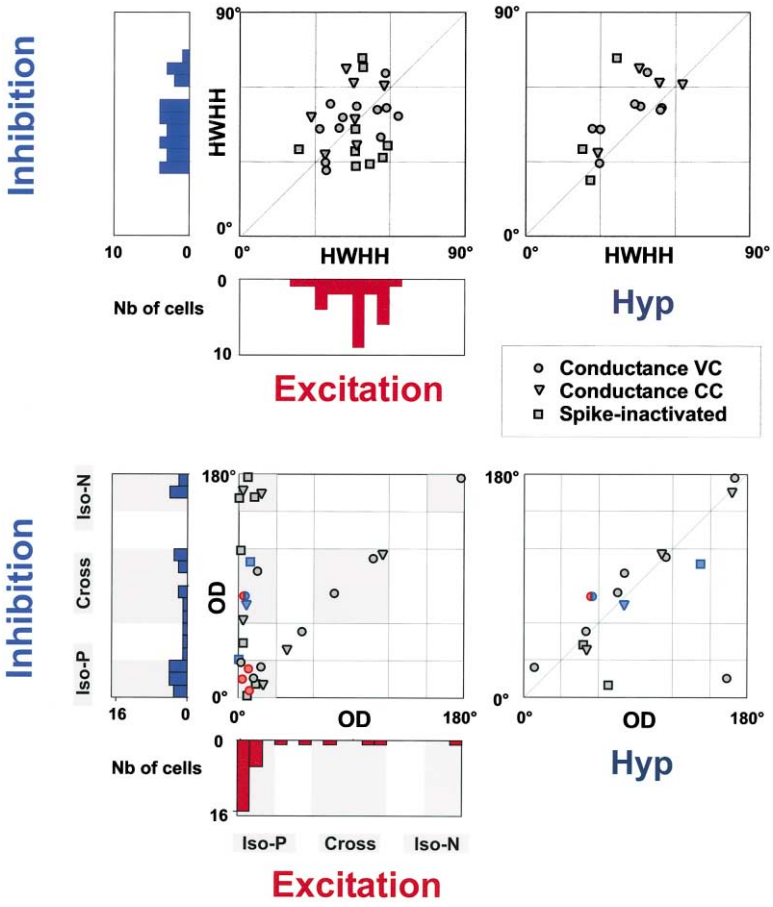

Figure 5. Excitatory and Inhibitory Input Tunings: Population Analysis

This figure compares the tuning characteristics (HWHH and OD) of excitation and inhibition, revealed by two different methods. In the scatter plots, circles represent cases where the excitatory and inhibitory conductance tunings were measured in VC (12 cases), triangles the cases where these were measured in CC (7 cases). Squares represent cells where the inhibitory selectivity was explored with the spike inactivation protocol (9 cases). In these cases, the tuning of the depolarizing component used to estimate that of excitatory input may partially mask the presence of excitatory input for nonpreferred directions. (Top left) The tuning width (HWHH) of inhibition is compared with that of excitation on a cell-to-cell basis. The distribution of the tuning width for each component is represented along the corresponding coordinate axis. (Top right) The tuning width of inhibition is compared with that of the hyperpolarizing component (*Hyp*). (Bottom) Similar plots of the optimal direction (OD) of inhibition versus that of excitation (left panel) or versus that of the hyperpolarizing component (right panel, *Hyp*). All direction preferences are expressed relative to that of the spike output. Filled red and blue symbols correspond, respectively, to the cases where excitatory or inhibitory orientation tuning was found to be statistically nonselective (index ratio lower than 0.10).

lus (NP-NP). These different combinations (among four theoretically possible) were associated with particular modes of temporal overlap between the excitatory and the inhibitory conductances.

In terms of *orientation selectivity* (summary in Table 1 and Figure 6), in about two thirds of the cells, both excitatory and inhibitory conductance tunings were biased toward the preferred orientation (P-P class: 10/16, 62%, see cells 10 and 11, Figure 4). The tuning widths of excitatory and inhibitory conductances were, on average, broader than that of the spike output but similar to that of the depolarization component (see Table 1 and Figure 6). On a cell-to-cell basis, however, the tuning widths of excitatory and inhibitory conductances were often different. The plot of the tuning width of excitation versus that of inhibition shown in Figure 5, indeed illustrates that few data points lie on the diagonal and that no particular tendency is observed. The excitatory and inhibitory conductance tuning widths in cell 10 (Figure 4) showed poor selectivity, but their temporal relationship (see cross-correlation graphs in Figure 4) was highly dependent on orientation (and direction): for the preferred direction, both conductances were in anti-phase (temporal overlap [TO] index of 27%), whereas for the nonpreferred orientations, they were in-phase (TO of 77%). This observation seems to be the general case for cells of the type P-P (TO: 36% $\pm$ 20% for preferred direction versus 71% $\pm$ 18% for nonpreferred orientations, paired $p < 0.01$, $n = 12$ [VC and CC recordings]).

For one fifth of the studied population (P-NP class: 3/16, 19%, see cell 12, Figure 4), the excitatory input was iso-oriented, and the inhibitory input was cross-oriented. The tuning width of inhibition was wider than for excitation, but both were wider than spike tuning (see

Figure 4. Excitatory and Inhibitory Conductances

This figure presents four examples of whole-cell patch recordings, where measures of excitatory and inhibitory conductances were made in VC and CC modes (cell 13), each panel illustrating one cell. Excitatory conductances are in red, and inhibitory conductances are in blue. Note that the scale of excitatory conductance is double that of the inhibitory conductance. The case of iso-oriented excitatory and inhibitory conductances is illustrated in cell 10 (Patch, Simple RF, OD: *Dep* 2°, *Hyp* 9°, *Gexc* 19°, *Ginh* 25°) and cell 11 (Patch, Simple RF, OD: *Dep* 2°, *Hyp* 169°, $1/\sigma$ 172°, *Gexc* 180°, and *Ginh* 179°). Both conductances were optimal in the preferred direction for cell 10 and in the null direction for cell 11. Cell 12 (Patch, Simple RF) illustrates the case of a cross-oriented inhibitory conductance with iso-oriented excitation (OD: *Dep* 10°, *Hyp* 8°, *Gexc* 6°, and *Ginh* 75°). Cell 13 (Patch: Complex RF) illustrates the case where both excitatory and inhibitory conductances were cross-oriented (OD: *Dep* 146°, *Hyp* 114°, *Gexc* 108°, and *Ginh* 111°). The bottom insets give the normalized cross-correlation function between the excitatory and inhibitory conductance waveforms, and the ordinate for a zero time delay is used to quantify the degree of temporal overlap (TO) between the two waveforms (see Experimental Procedures).

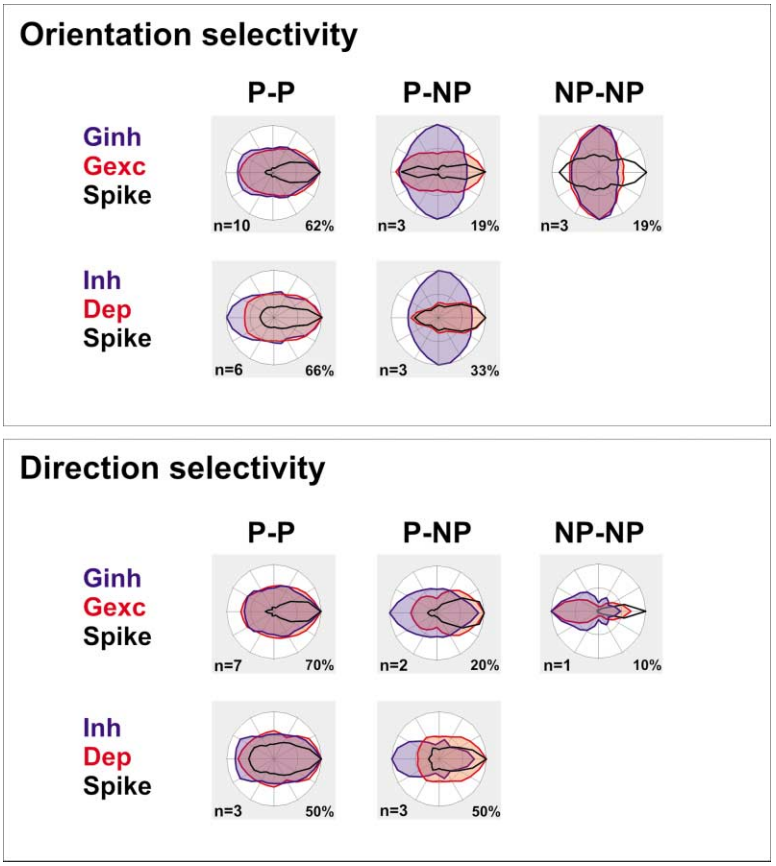

Figure 6. Diversity of Combinations between Excitatory and Inhibitory Input Tunings

(A) Averaged tunings of the excitatory and inhibitory inputs for cells grouped according to different schemes for orientation selectivity. Excitation-Inhibition: Preferred-Preferred (P-P), Preferred-Non Preferred (P-NP), Non preferred-Non preferred (NP-NP). The upper row of tuning curves is based on cells for which conductance measurements were made. In the lower row, tuning of the inhibition revealed in the spike-inactivated state can be compared with that of the depolarizing component observed at rest.

(B) Similar plots for the study of direction selectivity. Excitation-Inhibition: P-P (Iso-P-Iso-P), P-NP (Iso-P-iso-N), NP-NP (Iso-N-Iso-N).

Table 1 and Figure 6). A much higher level of temporal overlap between excitatory and inhibitory conductances was found than for the previous class of cells (P-P), independently of the orientation of the stimulus (Table 1).

In the remaining cells (NP-NP class: 3/16, 19%, see cell 13, Figure 4), excitatory and inhibitory conductances shared the same orientation preference, either oblique (1/16) or cross-oriented (2/16), distinct from the spike-based preference (see the diagonal of Figure 5). For these cells, the tuning width of excitatory and inhibitory orientation tuning was broad (see Table 1). As in the previous class, the two conductances were in temporal overlap (see Table 1). The orientation selectivity of spiking activity (output tuning) results mainly from the broader tuning of excitation (higher base value) that predominates over inhibition for orientations away from the initial input preference (see cell 13, Figure 4 and Table 1).

In terms of *direction selectivity*, cells with an iso-oriented excitation and inhibition have a highly direction selective spike output (DI $=$ 0.76 $\pm$ 0.25, n $=$ 10), whereas cells with nonoptimally tuned inhibition are much less direction selective. This applies for cells with only cross-oriented inhibition (DI $=$ 0.2, n $=$ 3) and for cells where both excitation and inhibition are cross-oriented (DI $=$ 0.23 $\pm$ 0.13, n $=$ 3). For simplicity and because cells with iso-oriented excitatory and inhibitory conductances present a high direction selectivity compared to others, only these cells (Iso-P or Iso-N) were considered for the study of direction selectivity. A classification for direction selectivity similar to that established for orientation preference was observed (summary in Table 2 and Figure 6).

A majority of cells showed both excitation and inhibition tuned to the preferred direction (P-P class: 7/10, 70%). These cells had a depolarizing response and input conductances with a lower direction selectivity index than that of the spiking output (see Table 2). The temporal overlap between excitatory and inhibitory conductances seems to play an important role for the spiking direction selectivity, the TO index being significantly lower for the preferred direction than for the null direction (TO: 29% $\pm$ 20% versus 61% $\pm$ 19%, $p < 0.01$, see Table 2).

Two cells had excitatory conductances tuned to the preferred direction and inhibitory conductances tuned to the null direction (P-NP class: 2/10, 20%). The spiking and depolarization components were both moderately direction selective, whereas excitatory and inhibitory conductance inputs were not (see Table 2). In contrast to the previous case, excitation and inhibition acted concomitantly, and the temporal overlap between excitatory and inhibitory conductances was equally high for both directions (see Table 2).

In the last cell, both excitatory and inhibitory inputs peaked for the null direction (NP-NP class: 1/10, 10%). The same two processes (relative tuning and temporal overlap) can account for the spike output selectivity. First, inhibition was more tuned to the null direction than excitation, in such a way that excitation still evoked a depolarization for the preferred direction that was larger than that for the null direction (see Table 2). Second,

Table 1. Orientation Selectivity of Excitatory and Inhibitory Conductances

		Gexc			Ginh			Pref	N-Pref	Dep.	Spike	
Schema	# Cells	PO	HWHH	Base	PO	HWHH	Base	TO	TO	HWHH	HWHH	DI
P-P	10/16	8° ± 6°	47° ±11°	31% ± 19%	17° ± 9°	47° ± 8°	27% ± 14%	36% ± 20%	71% ± 18%	47° ± 15°	26° ± 6°	0.76 ± 2
P-NP	3/16	7° ± 5°	38° ± 6°	38% ± 16%	82° ± 17°	53° ± 10°	43% ± 21%	85% ± 17%	94% ± 4%	41° ± 13°	24° ± 10°	0.23 ± 0.2
NP-NP	3/16	78° ± 34°	49° ± 14°	41% ± 10%	81° ± 24°	48° ± 16°	27% ± 10%	91% ± 17%	94% ± 5%	52° ± 24°	35° ± 12°	0.23 ± 0.1

PO, preferred orientation; HWHH, half width at half height; Base, Basal fraction; TO, temporal overlap; DI, directional selectivity index; Gexc and Ginh, excitatory and inhibitory conductances; Dep, depolarizing component; Pref, spike-based preferred orientation; Non-Pref, oblique or cross-orientation. See text for further details.

the temporal overlap between excitation and inhibition was much larger for the null (94%) than for the preferred direction (32%).

In addition, a strong correlation was observed between the waveforms of the inverse of trial-to-trial variability and of the inhibitory input conductance (example in Figure 4, cell 11; compare the green and blue traces). This correlation was also present in the polar plots for the two components.

We have extracted from the current-clamp and voltage-clamp recordings various measures that reflect to different extents the range and relative dominance of excitatory and inhibitory inputs to a cell. It is thus possible to compare the selectivity of subthreshold depolarizing and hyperpolarizing components measured at rest with the tuning of inhibitory and excitatory conductances. Nine cells in which input conductance dynamics were measured showed a significant hyperpolarizing response evoked at rest. The optimal orientation of the hyperpolarizing component was significantly correlated with that of the inhibitory conductance ($r^2 = 0.73$; $p < 0.01$ [$n = 12$]; see Figure 4). This suggests that the integral of the hyperpolarizing component, when detectable, gives a gross but nevertheless reliable estimation of the optimal orientation for the inhibitory input. The tuning width of the evoked hyperpolarizations was, on average, sharper than that of the inhibitory conductance (mean of the difference: $8° \pm 10°$). In contrast, the optimal orientation of the evoked depolarization was not significantly correlated with that measured for the excitatory conductance increase ($r^2 = 0.10$; n.s.). This implies, as illustrated in some examples (Figure 4: cells 11 and 13) that the optimal orientation of the excitatory input cannot be predicted from the integral of the evoked depolarization.

Discussion

This study represents a quantitative investigation of the role of the balance between excitation and inhibition in the emergence of orientation and direction selectivity in cat primary visual cortex. On the basis of conductance measurements, we report three different schemes of interaction between excitation and inhibition that underlie the genesis of orientation and direction selectivity.

For *orientation selectivity*, the P-P schema seems to be the most common. Sixty-two percent of the cells, for which excitatory and inhibitory synaptic conductances were measured, fell in this category. With the spike-inactivation method, we only have access to the selectivity of inhibition. However, as no NP-P cases were observed with conductance measurements, we can still classify cells with iso-oriented Inh component in the P-P schema (66% of cells). In contrast, the detection of significant evoked hyperpolarization or spike suppression for the preferred direction or orientation appear to be less sensitive indicators of the presence of iso-oriented inhibition, since these were noticeable in only a smaller proportion of cases (respectively, 40% and 33% of the cells). This discrepancy could result from the fact that, in some cells, excitation and inhibition are in temporal overlap for the preferred stimulus; therefore, their interaction will evoke a change in $1/\sigma$ without a

Table 2. Direction Selectivity of Excitatory and Inhibitory Conductances

		Gexc		Ginh		Pref.	N-Pref.	Dep	Spike
Schema	# Cells	PD	DI	PD	DI	TO	TO	DI	DI
P-P	7/10	9° ± 7°	0.22 ± 0.1	17° ± 8°	0.29 ± 0.3	29% ± 20%	61% ± 19%	0.28 ± 0.1	0.74 ± 0.2
P-NP	2/10	9° ± 9°	0.29 ± 0.1	167° ± 2°	−0.19 ± 0.2	91% ± 16%	92% ± 8%	0.60 ± 0.2	0.67 ± 0.4
NP-NP	1/10	179°	−0.2	180°	−0.36	32%	94%	0.65	1

This table concerns the subpopulation of cells where the optimal orientations for excitatory and inhibitory inputs are both iso-oriented (Iso-P and Iso-N). Pref, spike-based preferred direction; Non-Pref, Null direction. Same conventions as in Table 1. See text for further details.

hyperpolarization of the mean membrane potential (cell 5 in Figure 1). This interpretation is supported by the observation that 59% of the cells that showed a significant decrease of trial-to-trial variability without significant hyperpolarization (Figure 2, $1/\sigma$ only) exhibited a $1/\sigma$ component tuned for the preferred orientation. In cells where both excitatory and inhibitory conductances were measured, inhibitory tuning for nonpreferred orientations was observed in 38% of cases (P-NP schema, 19%; NP-NP, 19%). For the spike-inactivation protocol, 33% of cells had an inhibitory component tuned to a nonpreferred orientation (P-NP or NP-NP schemas). The other response components, hyperpolarization, spike suppression, and $1/\sigma$ (only), were tuned for nonpreferred orientations in, respectively, 60%, 66%, and 41% of cells.

In order to generalize our conclusions to the whole population of recorded cells, we extrapolated an estimate of the preferred orientation of the inhibitory input on the basis of the degree of correlation found between the different inhibitory-like components at rest (Hyp, Supp, $1/\sigma$) and the inhibitory component in the spike-inactivated state (Inh) or the inhibitory conductance (Ginh) when measured. The global picture remained the same as that established from the more restricted sample of conductance measurement: 60% of cells showed iso-oriented inhibition, and 40% of cells showed cross-oriented inhibition.

For *direction selectivity*, cells receiving a dominant inhibitory input or showing an optimal hyperpolarizing response for nonpreferred orientations were on average less direction selective than other cells (see Figures 2 and 6). Consequently, we considered only cells with an iso-oriented inhibitory-like component (i.e., either spike suppression, hyperpolarization, or inhibitory component tuned to the preferred orientation). In a majority of these cells (70% on the basis of conductance measurement, and 50% on the basis of the spike inactivation protocol), excitation and inhibition were tuned in the preferred direction (P-P schema). A comparable proportion of cells (60%) showed a hyperpolarizing component that was the largest for the preferred direction. In cells where synaptic conductances were measured, an inhibitory preference for the null direction was observed in 30% of cases (20% for P-NP and 10% for NP-NP schemas). When using the spike inactivation protocol, 50% of the cells showed inhibition tuned to a direction opposite to that of the spike preference (P-NP or NP-NP). In comparison 40% of cells exhibited a dominant hyperpolarization in the null direction.

In summary, our results argue against a single canonical circuitry underlying the genesis of receptive field properties within primary visual cortex. In the literature, the presence of inhibition evoked by nonpreferred stimuli has been a controversial issue, with contradictory conclusions reached by several teams using intracellular protocols. In fact, the diversity of combinations of excitatory and inhibitory inputs observed in our data does account for the wide range of observations that have been previously reported. Before proposing hypothetical scenarios of cortical organization, we will compare our findings with those established from previous works.

Spike and Depolarization

Similarly to two recent reports (Volgushev et al., 2000; Carandini and Ferster, 2000), we found that the tuning of depolarizing responses is, on average, wider than that of spike responses. However, as previously reported (Volgushev et al., 2000), we observed that the average difference masks a large diversity in the improvement in selectivity between the depolarizing component and the spike output. No correlation was found between this improvement and either the absolute or the relative spike threshold, but cells classified as receiving cross-oriented inhibition showed a significantly smaller improvement than those receiving iso-oriented inhibition. We conclude that the diversity in the tuning improvement reflects more the diversity in the combination of inputs than postsynaptic intrinsic properties.

Suppression and Hyperpolarization

The presence of cross-oriented suppression has already been demonstrated on the basis of extracellular recordings and stimulus interaction protocols (Bishop et al., 1973; DeAngelis et al., 1992; Ringach et al., 2002). Early intracellular studies in visual cortex (Benevento et al., 1972; Creutzfeldt et al., 1974; Innocenti and Fiore, 1974), whose findings were later replicated (Volgushev et al., 1993; Martinez et al., 2002), gave qualitative reports of diversity in the orientation tuning of visually evoked depolarizations and hyperpolarizations. In the present study, we present a quantitative analysis of the orientation and direction preference of the hyperpolarizing component explored over a large cell population based on explicit criteria of statistical significance. In addition, for some cells we have been able to compare the respective tunings of the depolarizing and hyperpolarizing components with those of the evoked inhibitory and excitatory conductance changes, which are expected to represent the actual synaptic input more faithfully. We observed a significant correlation between the optimal orientation of the inhibitory conductance and that of the hyperpolarizing component when detectable

at the resting state, suggesting that indeed some of the cells reported in previous works did receive a cross-oriented inhibition.

Trial-to-Trial Variability of the Membrane Potential

Although the trial-to-trial variability in the evoked response has been a focus of attention in many extracellular studies, it has been only rarely analyzed in intracellular studies. Our hypothesis, that the reduction of the trial-trial variability is produced by the presence of a strong input dominated by inhibition, has been addressed in this study in a variety of ways. In many cells, the $1/\sigma$ component in the membrane potential was found to be correlated with the presence of a significant evoked spike suppression and hyperpolarization. In other cells where a variability decrease was found concomitantly with a mean depolarization evoked at rest, the presence of inhibition was revealed during spike inactivation protocols (see cell 10). Furthermore, in cells recorded in voltage clamp, a strong decrease of variability was found to be correlated with a strong increase of the inhibitory conductance component (see cell 15).

The method used here takes into account the time course of the trial-to-trial variability stimulus locked waveform. It differs from the approach used previously by Anderson et al. (2000c), where the trial-to-trial variability was averaged over the stimulus presentation period and considered as "a noisy component varying little with contrast and orientation." However, despite averaging, their data did show a modulation on the order of 30% between preferred and cross-orientations, which is compatible with our own observations. From our results, we conclude that it is necessary to take into account the temporal waveform of the trial-to-trial variability for each orientation or direction in order to predict correctly the temporal spiking pattern on the basis of the mean visual response with a fixed threshold for spike initiation. We suggest that the addition of a constant noise, as proposed in the model of Anderson et al. (2000c), can only be relevant at the conductance level: the visually evoked dynamics of the mean global conductance modulates the trial-to-trial membrane potential variability.

The spiking responses evoked in vivo are extremely variable from trial to trial (Heggelund and Albus, 1978; Dean, 1981). Nevertheless, a recent study (Mechler et al., 1998) shows that this variability depends on the type of stimuli used: drifting edges (transient stimuli) but not gratings (steady-state stimuli) generate responses with reproducible stimulus-dependent changes in the temporal structure of the spike train (temporal coding). In agreement with this study, we observed, using transient stimuli, the presence of reproducible stimulus-dependent changes in the trajectory of membrane potential, which affect the temporal structure of the spike train.

Unmasking Inhibition by Current Injection

One possible way to detect inhibition in vivo is to study the voltage dependence of the evoked response through current injection (Innocenti and Fiore, 1974). The use of depolarizing currents to enhance the visibility of inhibition was applied in the earlier work of Ferster (1986) and Sato et al. (1991). Both groups concluded on the basis of a limited sample that the evoked hyperpolarization during positive current injection and the evoked depolarization with no current shared the same orientation preference and selectivity without quantifying the tuning curves of the detected inhibition. The reference criterion used in the present study was to use a current strong enough to produce the total inactivation of the action potential, thus abolishing contamination by spiking activity. At this current injection level, evoked depolarizations were suppressed, and only hyperpolarizations could be detected. This indicates that the cell membrane potential was maintained close to the reversal potential of excitatory synapses, thus minoring a possible masking of inhibitory components by NMDA-dependent responses that may dominate at intermediate levels of depolarization.

Excitatory and Inhibitory Conductance Tuning

The present data confirm our previous observation that visual stimulation evokes strong conductance increases (Borg-Graham et al., 1998). The relative change in peak conductance (around 110%) is similar to values found by Anderson et al. (128%). We also observed that the maximal conductance increase was quite variable from cell to cell.

Our method of conductance decomposition differs partly from that of Anderson et al. (2000b). We decomposed the conductance into three components, excitation, inhibition dominated by chloride conductance (reversal potential of -80mV), and by potassium conductance (-95mV) instead of two components with an intermediate value for the reversal potential of the inhibition (-85mV in Anderson et al., 2000b). This method tends to avoid both underestimating the chloride conductance and obtaining a negative value for the excitatory conductance. Moreover, we estimated the total synaptic conductance, both evoked and spontaneous, based on an estimation of the leak conductance, whereas Anderson et al. (2000b) derived only the evoked synaptic conductance increase. This allowed us to detect significant changes in the balance between the excitatory and inhibitory conductances, even with small absolute evoked conductance increases.

Both the two-term decomposition method used by Anderson et al. (2000b) and the three-term decomposition method used here do not take into account possible nonlinearities introduced by NMDA receptor activation. Nevertheless, taking into account numerous immunoanatomical reports suggesting that, in neocortical neurons, inhibitory synapses are located more proximal to the soma than excitatory synapses, it seems unlikely that NMDA conductances mask inhibitory conductances, although the reverse situation may be true.

Using drifting gratings in conjunction with current-clamp recordings, Anderson et al. (2000b) concluded on the basis of steady-state responses that conductance was invariably maximal for a stimulus of the preferred orientation. These authors also concluded that orientation preference and tuning width on a cell-by-cell basis were similar for both excitatory and inhibitory input conductances. One reason for these apparent discrepancies with the present findings may be linked to differences in the fitting methods. In Anderson et al. (2000b), in order to minimize the number of parameters,

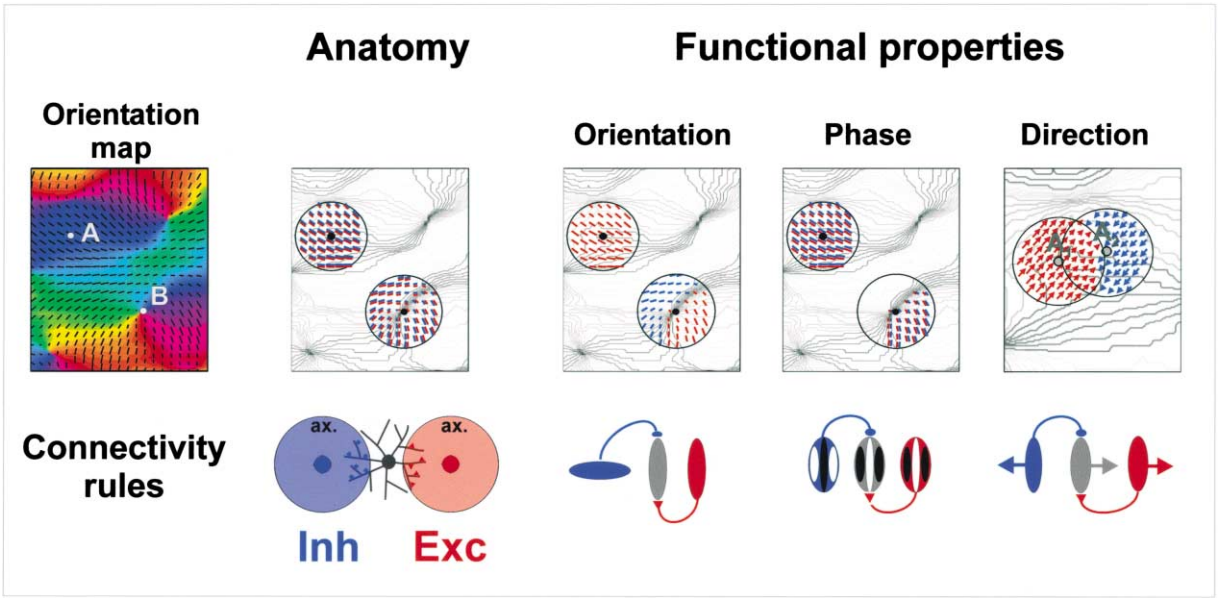

Figure 7. Principles for Generating Diversity

Connectivity principles applied in different locations of the cortical orientation/direction maps. (Upper row, left panel) Iso-oriented domain (A) and pinwheel centers (B). (Upper row, right panel) Iso-directional domain (A1) and demarcation line between two opposite iso-directional domains (A2). Excitatory cells are in red, inhibitory cells in blue, and the target cell in gray. (Lower row) The left panel illustrates connectivity rules based on the anatomy: the intracortical connectivity distribution is governed only by the distance between cortical sites. The extent of the axon (ax.) afferent to a given postsynaptic cortical cell is schematized by a disk. The right panel illustrates connectivity rules based on functional correlation, with, respectively, excitatory and inhibitory synapses connecting cells with similar or dissimilar receptive field properties. Receptive field properties are symbolized by an oriented ellipse for Orientation selectivity, by a Gabor patch for Spatial Phase, and by an arrow for Direction selectivity. See text for further details. The schematized direction map was derived from the orientation map kindly provided with the courtesy of F. Chavane and A. Grinvald, Weizmann Institute of Science.

the mean and modulation of the input conductance were fitted together, forcing them to peak at the same orientation with the same tuning width. However, it is apparent in some of their examples that this constraint can lead to poor fits and that the respective tunings of the modulation and of the mean are uncorrelated (see, for instance, Figure 10 in Anderson et al. [2000b]: in cells 1 and 6, the increases in mean conductance are clearly cross-oriented with the spike preference, whereas the modulation of conductance is iso-oriented). Thus, in spite of the apparent opposition between the conclusions of Anderson et al. (2000b) and our own, diversity in conductance tuning seems equally present in both studies. Differences in fact concern more quantitative issues: Anderson et al. (2000b) concluded that the orientation tuning width is narrow and identical for excitation and inhibition (HWHH: 22°), whereas we report here that the tunings of excitation and inhibition are larger and less selective (HWHH: 45°; base: 30%). We found also that the respective tuning widths of excitation and inhibition differ on a cell-to-cell basis (Figure 5), although these values averaged across all cells are comparable.

Principles for Generating Diversity

In summary, we conclude that, depending on the recorded cell, orientation and direction selectivity stem from a variety of combinations of excitatory and inhibitory synaptic tuning. We discuss below the implications of these findings for theoretical issues regarding the computational role of the visual cortical network architecture. Our data suggest that various computational solutions could be implemented locally and might coexist in the same network. We propose simple local connectivity rules based on neighborhood relationships that, applied to the whole network, could explain such diversity.

Functional cortical maps of orientation selectivity present a high level of spatial heterogeneity, with pinwheel loci exhibiting high spatial gradients in orientation preference, and iso-orientation domains with low orientation gradients (Bonhoeffer et al., 1995). However, whatever their positions within this heterogeneous map, cells present a high level of orientation selectivity (Maldonado et al., 1997). If we consider that intracortical connectivity distribution is governed mainly by the distance between cortical sites (Das and Gilbert, 1999), cells located at the pinwheel centers (position B, Figure 7) should receive a much broader range of orientation tuned input than cells in the middle of iso-orientation domains (position A, Figure 7). This will create a first source of diversity, between cells receiving mainly inputs tuned to the same orientation and cells receiving inputs from a wide range of distinct orientation domains. In addition, differences between excitatory and inhibitory input selectivities can arise from the different extents of the axonal and dendritic arborizations of excitatory and inhibitory neurons (Somers et al., 1995; McLaughlin et al., 2000).

A second source of diversity in the cortical network could result from the shaping of intracortical connectiv-

ity by activity-dependent processes. Both theoretical models and experimental data suggest that correlated pre- and postsynaptic activities stabilize and strengthen the gain of excitatory connections and that uncorrelated activities reinforce inhibitory connections (review in Frégnac, 2002). Therefore, cells with similar multidimensional functional preference (orientation, direction, phase, and spatial frequency) will tend to excite each other reciprocally. In contrast, cells which differ in at least one of these functional preferences will inhibit each other. The final connectivity state stabilized in adult cortex will be the result of a local synaptic plasticity principle applied for various dimensions of the visual stimulus. It should be noted that in this correlation-based framework, the source of the anisotropy (thalamocortical versus intracortical) cannot be identified, since it will be propagated through synaptic changes distributed across the whole network.

If we apply these hypothetical rules of plasticity to the *orientation selectivity* domain and the intracortical connectivity pattern defined previously, then cells located in the center of an iso-orientation domain will receive iso-oriented excitation from cells sharing similar receptive field properties and inhibitory input from iso-oriented cells which differ in their phase or spatial frequency selectivity (akin to the push-pull model). The same reasoning predicts that cells located near pinwheel centers will receive, in addition, inhibition from cells which differ in their orientation preference from the target cell (hence, oblique and cross-oriented input). In comparison, the model of Troyer et al. (1998), based on correlation rules dependent on the spatial phase between subfields, only considers excitatory and inhibitory connections between cells which share the same orientation preference and does not generalize the plasticity principle to the orientation domain. According to our generalized schema, inhibitory connectivity between neurons from different orientation columns provides a simple solution that will produce contrast invariance for both excitatory and inhibitory neurons (see also Adorjan et al., 1999).

For *direction selectivity*, the same reasoning can be applied. Optical maps established for direction preference show that iso-orientation domains appear divided into two contiguous regions exhibiting preferences for opposite directions (Shmuel and Grinvald, 1996; Kisvarday et al., 2001). Cells close to the separation line will receive inhibitory inputs tuned to the preferred direction, whereas cells away from this line will receive only iso-preference inhibition. If, as predicted by our organization principle, cells near pinwheel centers receive cross-oriented inhibition, our data suggest in addition that these cells have weak direction selectivity.

This qualitative model, which accounts for part of our results, underscores sources of diversity. Restricting test stimulations to a spot or a contrast edge may significantly reduce the identification of visual signals that contribute or have contributed in the past to correlated activity in the cortical network. For example, center-surround experiments show the fact that at least some cells in the visual cortex respond maximally for cross-oriented bipartite stimuli, independently of the actual orientation of the stimulus (Sillito et al., 1995), in spite of the fact that they express normal orientation selectivity when tested with classical stimuli. This might explain our apparent paradoxical observation that some cells receive excitatory and inhibitory input for what we defined as nonoptimal stimuli on the sole basis of a light bar stimulus. It may be that, with different stimulus configurations or dimensions, the evoked synaptic input and the corresponding spike output might indeed share a similar specificity, with the connectivity obeying the same organization principle.

The arguments that we have presented so far concern the dependency of the input distribution on the location of the cell in the orientation and direction selective network, as visualized by optical imaging of superficial layers. Another source of input variability may be linked with the laminar position of the cell within the depth of the cortical column. A recent study combining intracellular recordings and biocytin labeling reports that the tuning preference of the hyperpolarizing component is correlated with the laminar location of cells (Martinez et al., 2002), inhibition being dominantly iso-oriented for granular and supragranular layers, and often exhibiting a cross-oriented preference in deep layers, most specifically in layer V. These authors conclude that this diversity in the inhibitory tuning seen across the cortical depth reflects hierarchical levels of integration in the serial flow of cortical processing. We propose here that the noticeable difference found between supragranular and granular layers on the one hand and infragranular layers on the other hand could simply reflect a diversity in the input sampling in the laminar plane (Buzas et al., 2001; Kisvarday et al., 1994; Yousef et al., 1999).

In summary, the diversity of input combinations found across cells may reflect anatomical nonhomogeneities in the lateral intracortical connectivity pattern. This diversity could result from topological irregularities in the layout of the orientation preference map, and its functional impact may be up- and downregulated by correlation-based activity-dependent processes. In favor of our view, several optical mapping experiments have shown that the position of the cell in the orientation map may influence the amplitude of the orientation change produced by a fixed orientation adaptation protocol (Dragoi et al., 2001; Schuett et al., 2001). We propose here that these regional anisotropies in plasticity in the developing cortex, or adaptation in the adult cortex, in fact reflect the regional dominance of different computational schemas for the genesis of orientation preference.

Experimental Procedures

Cells in the primary visual cortex of anaesthetized (Althesin) and paralyzed cats (for details on the surgical preparation, see Bringuier et al., 1997, 1999) were recorded intracellularly using an Axoclamp 2A amplifier. Sharp electrode recordings (39 cells) were performed in bridge mode with 55–90 MΩ glass pipettes filled with 2 M potassium methyl sulfate and 4 mM potassium chloride. The average resting membrane potential was −67.5mV ± 5mV. Whole-cell patch recordings (49 cells) were made with 3–5 MΩ glass patch electrodes filled with a solution containing 140 mM K-gluconate, 10 mM HEPES, 4 mM ATP, 4 mM $MgCl_2$, 0.4 mM GTP, and 0.5 mM EGTA (KOH), with pH adjusted to 7.3 with KOH, and the osmolarity adjusted to 285 mosM. The seal resistance in attached mode was always above 1 GΩ. In whole-cell mode, the average resting potential was −66.5mV ± 6mV. In voltage-clamp recordings, the access resistance was always lower than 40 MΩ. The estimate of access resis-

tance was revised as necessary over the course of the experiment and, in some cases, off-line, by fitting the response to subthreshold hyperpolarizing current steps to the sum of two exponentials. A tip offset potential of 10mV was subtracted from the voltage records off-line.

Data processing and visual stimulation protocols were done using in-house software (Gérard Sadoc, Acquis1-Elphy, Biologic CNRS-UNIC/ANVAR). Three-millimeter artificial pupils were used, and appropriate corrective optical lenses were added. The receptive field of each cell was quantitatively characterized using a sparse noise mapping. Receptive fields were classified as Simple or Complex using classical criteria on the space-time separation between On and Off responses, including subdivision into S1 and C1 complex types for unimodal receptive fields, according to the presence or absence of antagonist hyperpolarization. Orientation and direction tuning curves were measured with moving bars (direction of motion perpendicular to orientation) swept across the full extent of the subthreshold receptive field, and using random sequences of 8 or 12 directions (angular step: 45° and 30°, respectively) repeated ten times.

For data analysis, we extracted the respective orientation and direction tuning curves of the following response components: spiking activity and spike suppression, membrane potential depolarization and hyperpolarization (without injection of current and during spike inactivation), trial-to-trial variability of the membrane potential and excitatory and inhibitory conductances. For the suprathreshold activity, PSTHs were computed with a 25 ms bin width, and the spike increase and spike suppression components were defined as the integral of firing rate, respectively, above and below the mean pre-trigger background firing rate. For subthreshold activity, spike events were removed from the raw record, and membrane potential was interpolated before and after each spike occurrence. The depolarizing and hyperpolarizing evoked components were defined on the basis of a quantitative amplitude selection criterion as the integral of voltage, respectively, above and below the mean depolarizing and hyperpolarizing fluctuations in the resting potential measured during spontaneous activity. Trial-to-trial variability was calculated as the inverse of the standard deviation ($1/\sigma$) of the time course of the stimulus-locked membrane potential response over all stimulation trials. The $1/\sigma$ component was defined by the integral above the mean background value. The $1/\sigma$ waveform is expressed as the percentage of change from the spontaneous reference level. Measurement of enhanced hyperpolarizations were made in a sample of cells recorded with sharp electrodes while applying depolarizing current sufficient to fully inactivate Na^+ spike currents. The quantification methods used in the spike-inactivated state were the same as those applied from the resting state. To determine if responses calculated over the whole period of visual stimulation were significant, the mean of each component, defined by its integral normalized by the effective time during which its presence was detected (see above amplitude selection criterion), was compared with the normalized mean of this component during spontaneous activity, using a Student's t test. For polar plot measurements, the spontaneously expected component value was subtracted from the evoked component.

For whole-cell patch-clamp recordings, the dynamics of the input conductance and its associated composite reversal potential were measured as described previously (Borg-Graham et al., 1998). In order to address the significance of the conductance measurement, a nonparametric bootstrap method was used, similar to that applied by Anderson et al. (2000b). The conductance waveform was decomposed to give the sum of a leak conductance (G_{leak}) and a global synaptic conductance (G_{syn}). G_{leak} was estimated as the lower boundary of the conductance waveform at rest and given by the threshold value corresponding to the 1% percentile of the cumulative distribution of conductance measures during spontaneous activity. The reversal potential E_{leak} was assumed to be in the order of −80mV (Paré et al., 1998). The synaptic conductance term was further linearly decomposed into three conductance components corresponding to the activation of one type of excitatory synapse and two types of inhibitory synapses, each associated with known, fixed reversal potentials. The value of the reversal potential of $GABA_A$ receptor activation was measured by pharmacologically blocking other synaptic components in a slice preparation of rat visual cortex and estimated at −80mV ± 3mV (n = 20). The other reversal potentials were fixed to 0mV for excitatory and −95mV for potassium conductances (associated with $GABA_B$ receptors).

We made the additional hypothesis that, depending on the actual value of the composite synaptic reversal potential, one or two out of three possible types of inputs contribute in a dominant manner to synaptic activation. Between 0mV and −80mV, the synaptic conductance can be decomposed into excitatory and $GABA_A$ conductances, and between −80mV and −95mV, into $GABA_A$ and $GABA_B$ conductances. Above 0mV and below −95mV, the synaptic conductance is thus equal, respectively, only to the excitatory or the potassium.

Similarly to the other measured components of the visual response, the evoked excitatory and inhibitory conductance components are given by the integral of the excitatory and inhibitory conductances above their mean values, calculated during pre-trigger and spontaneous activity. In order to determine the phase relationship and the degree of temporal overlap between excitation and inhibition, a normalized cross-correlation function was calculated between the two stimulus-locked excitatory and inhibitory conductance waveforms. An index representative of the temporal overlap (TO) is given by the cross-correlation "contrast" ratio, defined as the difference between the amplitude at time 0 and the amplitude at the peak of the cross-correlation function, divided by the difference between the maximum and the minimum of the cross correlation function.

The mean of each component during spontaneous activity was then subtracted from the visual evoked response. Orientation and direction tuning curves were calculated when response components, for at least one direction, passed a preset significance level ($p < 0.01$) based on either paired t tests or, in the case of conductance, on the bootstrap method. All components were averaged over the duration of the visual stimulation. Peak responses were calculated over a 25 ms bin. Direction tuning curves were fitted independently for each component by the sum of two Gaussians with the same width, whose peaks were 180° apart. The peak of the Gaussian determines the preferred (PD for spike output) or optimal direction (OD for other components). The half-width of the tuning curve at half the height (HWHH) of the peak is given by the standard deviation of the Gaussian multiplied by sqr(2. Ln2). The direction selectivity index (DI), which is independent of the fitting procedure, was defined as the difference in the responses obtained with stimuli of preferred and opposite directions, divided by the sum of those responses.

We also applied a spectral quantification method (S.D.O. analysis in Wörgötter and Eysel [1987]) which allows independent estimation of orientation and direction preferences and the computation of a selectivity index. An orientation index value of 0.1 or greater indicated that the circular distribution of the cell responses to moving stimuli was nonrandom ($p < 0.005$; Rayleigh test in Thompson et al., 1994; Zar, 1974). For tunings, a bootstrap method was applied to ensure that the standard deviation in the preferred orientation estimates ranged between 1° to 9° for the excitatory and inhibitory conductance components, depending on the cell and its tuning selectivity, i.e., well below the discretization step used for orientation and direction distributions.

Acknowledgments

This work was supported by grants from the Centre National de la Recherche Scientifique (CNRS) (Bioinformatique 00N25/0003, CTI01-55), the Fondation de France, the European Commission (IST-2001-34712), and Human Frontier Science Program (HFSP) RG-103-98 to Y.F. We thank Dr. Kirsty Grant for critical reading and Gérard Sadoc for continuous improvement of the intracellular analysis software package.

Received: May 9, 2002
Revised: December 16, 2002

References

Adorjan, P., Levitt, J.B., Lund, J.S., and Obermayer, K. (1999). A model for the intracortical origin of orientation preference and tuning in macaque striate cortex. Vis. Neurosci. *16*, 303–318.

Ahmed, B., Anderson, J.C., Douglas, R.J., Martin, K.A.C., and Nelson, J.C. (1994). Polyneuronal innervation of spiny stellate neurons in cat visual cortex. J. Comp. Neurol. *341*, 39–49.

Anderson, J., Lampl, I., Reichova, I., Carandini, M., and Ferster, D. (2000a). Stimulus dependence of two-state fluctuations of membrane potential in cat visual cortex. Nat. Neurosci. *3*, 617–621.

Anderson, J.S., Carandini, M., and Ferster, D. (2000b). Orientation tuning of input conductance, excitation, and inhibition in cat primary visual cortex. J. Neurophysiol. *84*, 909–926.

Anderson, J.S., Lampl, I., Gillespie, D.C., and Ferster, D. (2000c). The contribution of noise to contrast invariance of orientation tuning in cat visual cortex. Science *290*, 1968–1972.

Ben-Yishai, R., Bar-Or, R.L., and Sompolinsky, H. (1995). Theory of orientation tuning in visual cortex. Proc. Natl. Acad. Sci. USA *92*, 3844–3848.

Benevento, L.A., Creutzfeldt, O.D., and Kuhnt, U. (1972). Significance of intracortical inhibition in the visual cortex. Nature *238*, 124–126.

Berman, N.J., Douglas, R.J., Martin, K.A.C., and Whitteridge, D. (1991). Mechanisms of inhibition in cat visual cortex. J. Physiol. *440*, 697–722.

Bishop, P.O., Coombs, J.S., and Henry, G.H. (1973). Receptive fields of simple cells in the cat striate cortex. J. Physiol. *231*, 31–60.

Bonhoeffer, T., Kim, D.-S., Malonek, D., Shoham, D., and Grinvald, A. (1995). Optical imaging of the layout of functional domains in area 17 and across the area 17/18 border in cat visual cortex. Eur. J. Neurosci. *7*, 1973–1988.

Borg-Graham, L.J. (2001). The computation of directional selectivity in the retina occurs prior to the ganglion cell. Nat. Neurosci. *4*, 176–182.

Borg-Graham, L., Monier, C., and Frégnac, Y. (1996). Voltage-clamp measurement of visually evoked conductances with whole-cell patch recordings in primary visual cortex. J. Physiol. (Paris) *90*, 185–188.

Borg-Graham, L.J., Monier, C., and Frégnac, Y. (1998). Visual input evokes transient and strong shunting inhibition in visual cortical neurons. Nature *393*, 369–373.

Bringuier, V., Frégnac, Y., Baranyi, A., Debanne, D. and Shulz, D. (1997). Synaptic origin and stimulus dependency of neuronal oscillatory activity in the primary visual cortex of the cat. J. Physiol. *500*, 751–774.

Bringuier, V., Chavane, F., Glaeser, L., and Frégnac, Y. (1999). Horizontal propagation of visual activity in the synaptic integration field of area 17 neurons. Science *283*, 695–699.

Bush, P.C., and Sejnowski, T.J. (1994). Effects of inhibition and dendritic saturation in simulated neocortical pyramidal cells. J. Neurophysiol. *71*, 2183–2193.

Buzas, P., Eysel, U.T., Adorjan, P., and Kisvarday, Z.F. (2001). Axonal topography of cortical basket cells in relation to orientation, direction, and ocular dominance maps. J. Comp. Neurol. *437*, 259–285.

Carandini, M., and Ferster, D. (2000). Membrane potential and firing rate in cat primary visual cortex. J. Neurosci. *20*, 470–484.

Creutzfeldt, O.D., Kuhnt, V., and Benevento, L.A. (1974). An intracellular analysis of visual cortical neurons to moving stimuli: responses in a co-operative neuronal network. Exp. Brain Res. *21*, 251–274.

Crook, J.M., Kisvarday, Z.F., and Eysel, U.T. (1997). GABA-induced inactivation of functionally characterized sites in cat striate cortex: effects of orientation tuning and direction selectivity. Vis. Neurosci. *14*, 141–158.

Crook, J.M., Kisvarday, Z.F., and Eysel, U.T. (1998). Evidence for a contribution of lateral inhibition to orientation tuning and direction selectivity in cat visual cortex: reversible inactivation of functionally characterized sites combined with neuroanatomical tracing techniques. Eur. J. Neurosci. *10*, 2056–2075.

Das, A., and Gilbert, C.D. (1999). Topography of contextual modulations mediated by short-range interactions in primary visual cortex. Nature *399*, 655–661.

Dean, A.F. (1981). The variability of discharge of simple cells in the cat striate cortex. Exp. Brain Res. *44*, 437–440.

DeAngelis, G.C., Robson, J.G., Ohzawa, I., and Freeman, R.D. (1992). Organization of suppression in receptive fields of neurons in cat visual cortex. J. Neurophysiol. *68*, 144–163.

Douglas, R.J., Martin, K.A.C., and Whitteridge, D. (1988). Selective responses of visual cortical cells do not depend on shunting inhibition. Nature *332*, 642–644.

Douglas, R.J., Martin, K.A.C., and Whitteridge, D. (1991). An intracellular analysis of the visual responses of neurones in cat visual cortex. J. Physiol. *440*, 659–696.

Douglas, R.J., Koch, C., Mahowald, M.A., Martin, K.A.C., and Suarez, H.H. (1995). Recurrent excitation in neocortical circuits. Science *269*, 981–985.

Douglas, R., Koch, C., Mahowald, M., and Martin, K. (1999). The role of recurrent excitation in neocortical circuits. In Cerebral Cortex: Models of Cortical Circuits, P.S. Ulinsky, E.G. Jones, and A. Peters, eds. (New York: Kluwer Academic: Plenum Publishers), pp. 251–282.

Dragoi, V., Rivadulla, C., and Sur, M. (2001). Foci of orientation plasticity in visual cortex. Nature *411*, 80–86.

Eysel, U.T., and Shevelev, I.A. (1994). Time-slice analysis of inhibition in cat striate cortical neurones. Neuroreport *5*, 2033–2036.

Eysel, U.T., Crook, J.M., and Machemer, H.F. (1990). GABA-induced remote activation reveals cross-orientation inhibition in the cat striate cortex. Exp. Brain Res. *80*, 626–630.

Ferster, D. (1986). Orientation selectivity of synaptic potentials in neurons of cat primary visual cortex. J. Neurosci. *6*, 1284–1301.

Ferster, D., and Jagadeesh, B. (1992). EPSP-IPSP interactions in cat visual cortex studied with *in vivo* whole-cell patch recording. J. Neurosci. *12*, 1262–1274.

Ferster, D., and Koch, C. (1987). Neuronal connections underlying orientation selectivity in cat visual cortex. Trends Neurosci. *10*, 487–492.

Ferster, D., and Miller, K.D. (2000). Neural mechanisms of orientation selectivity in the visual cortex. Annu. Rev. Neurosci. *23*, 441–472.

Frégnac, Y. (2002). Hebbian synaptic plasticity. In The Handbook of Brain Theory and Neural networks, 2nd edition, M. Arbib, ed. (Boston, MA: MIT Press), pp. 512–522.

Heggelund, P., and Albus, K. (1978). Response variability and orientation descrimination of single cells in striate cortex of cat. Expl. Brain Res. *32*, 197–211.

Hirsch, J.A., Alonso, J.M., Reid, R.C., and Martinez, L.M. (1998). Synaptic integration in striate cortical simple cells. J. Neurosci. *18*, 9517–9528.

Hubel, D.H., and Wiesel, T.N. (1962). Receptive fields, binocular interaction and functional architecture in the cat's visual cortex. J. Physiol. *160*, 106–154.

Innocenti, G.M., and Fiore, L. (1974). Post-synaptic inhibitory components of the responses to moving stimuli in area 17. Brain Res. *80*, 122–126.

Kisvarday, Z.F., Kim, D.S., Eysel, U.T., and Bonhoeffer, T. (1994). Relationship between lateral inhibitory connections and the topography of the orientation map in cat visual cortex. Eur. J. Neurosci. *6*, 1619–1632.

Kisvarday, Z.F., Buzas, P., and Eysel, U.T. (2001). Calculating direction maps from intrinsic signals revealed by optical imaging. Cereb. Cortex *11*, 636–647.

Maldonado, P.E., Godecke, I., Gray, C.M., and Bonhoeffer, T. (1997). Orientation selectivity in pinwheel centers in cat striate cortex. Science *276*, 1551–1555.

Martinez, L.M., Alonso, J.M., Reid, R.C., and Hirsch, J.A. (2002). Laminar processing of stimulus orientation in cat visual cortex. J. Physiol. *540*, 321–333.

McLaughlin, D., Shapley, R., Shelley, M., and Wielaard, D.J. (2000). A neuronal network model of macaque primary visual cortex (V1): orientation selectivity and dynamics in the input layer 4Calpha. Proc. Natl. Acad. Sci. USA *97*, 8087–8092.

Mechler, F., Victor, J.D., Purpura, K.P., and Shapley, R. (1998). Robust temporal coding of contrast by V1 neurons for transient but not for steady-state stimuli. J. Neurosci. *18*, 6583–6598.

Nelson, S., Toth, L., Sheth, B., and Sur, M. (1994). Orientation selectivity of cortical neurons during intracellular blockade of inhibition. Science *265*, 774–777.

Paré, D., Shink, E., Gaudreau, H., Destexhe, A., and Lang, E. (1998). Impact of spontaneous synaptic activity on the resting properties of cat neocortical pyramidal neurons *in vivo*. J. Neurophysiol. *79*, 1450–1460.

Ringach, D.L., Bredfeldt, C.E., Shapley, R.M., and Hawken, M.J. (2002). Suppression of neural responses to non-optimal stimuli correlates with tuning selectivity in macaque V1. J. Neurophysiol. *87*, 1018–1027.

Roerig, B., and Kao, J.P. (1999). Organization of intracortical circuits in relation to direction preference maps in ferret visual cortex. J. Neurosci. *19*, RC44.

Ruff, P.I., Rauschecker, J.P., and Palm, G.A. (1987). Model of direction-selective "simple" cells in the visual cortex based inhibition asymmetry. Biol. Cybern. *57*, 147–157.

Sabatini, S.P., and Solari, F. (1999). An architectural hypothesis for direction selectivity in the visual cortex: the role of spatially asymmetric intracortical inhibition. Biol. Cybern. *80*, 171–183.

Sato, H., Daw, N.W., and Fox, K. (1991). An intracellular recording study of stimulus-specific response properties in cat area 17. Brain Res. *544*, 156–161.

Schuett, S., Bonhoeffer, T., and Hubener, M. (2001). Pairing-induced changes of orientation maps in cat visual cortex. Neuron *32*, 325–337.

Schummers, J., Marino, J., and Sur, M. (2002). Synaptic integration by V1 neurons depends on location within the orientation map. Neuron *36*, 969–978.

Sclar, G., and Freeman, R.D. (1982). Orientation selectivity in the cat's striate cortex is invariant with stimulus contrast. Exp. Brain Res. *46*, 457–461.

Shmuel, A., and Grinvald, A. (1996). Functional organization for direction of motion and its relationship to orientation maps in cat area 18. J. Neurosci. *16*, 6945–6964.

Sillito, A.M. (1979). Inhibitory mechanisms influencing complex cell orientation selectivity and their modification at high resting discharge levels. J. Physiol. *289*, 33–53.

Sillito, A.M., Kemp, J.A., Milson, J.A., and Berardi, N. (1980). A reevaluation of the mechanism underlying simple cell orientation selectivity. Brain Res. *194*, 517–520.

Sillito, A.M., Grieve, K.L., Jones, H.E., Cudeiro, J., and Davis, J. (1995). Visual cortical mechanisms detecting focal orientation discontinuities. Nature *378*, 492–496.

Somers, D.C., Nelson, S.B., and Sur, M. (1995). An emergent model of orientation selectivity in cat visual cortical simple cells. J. Neurosci. *15*, 5448–5465.

Thompson, K.G., Leventhal, A.G., Zhou, Y.F., and Liu, D. (1994). Stimulus dependence of orientation and direction sensitivity of cat LGNd relay cells without cortical inputs: a comparison with area 17 cells. Vis. Neurosci. *11*, 939–951.

Troyer, T.W., Krukowski, A.E., Priebe, N.J., and Miller, K.D. (1998). Contrast-invariant orientation tuning in cat visual cortex: thalamocortical input tuning and correlation-based intracortical connectivity. J. Neurosci. *18*, 5908–5927.

Volgushev, M., Pei, X., Vidyasagar, T.R., and Creutzfeldt, O.D. (1993). Excitation and inhibition in orientation selectivity of cat visual cortex neurons revealed by whole-cell recordings *in vivo*. Vis. Neurosci. *10*, 1151–1155.

Volgushev, M., Pernberg, J., and Eysel, U.T. (2000). Comparison of the selectivity of postsynaptic potentials and spike responses in cat visual cortex. Eur. J. Neurosci. *12*, 257–263.

Wörgötter, F., and Eysel, U.T. (1987). Quantitative determination of orientational and directional components in the response of visual cortical cells to moving stimuli. Biol. Cybern. *57*, 349–355.

Wörgötter, F., and Koch, C. (1991). A detailed model of the primary visual pathway in the cat: comparison of afferent excitatory and intracortical inhibitory connection schemes for orientation selectivity. J. Neurosci. *11*, 1959–1979.

Yousef, T., Bonhoeffer, T., Kim, D.S., Eysel, U.T., Toth, E., and Kisvarday, Z.F. (1999). Orientation topography of layer 4 lateral networks revealed by optical imaging in cat visual cortex (area 18). Eur. J. Neurosci. *11*, 4291–4308.

Zar, J.H. (1974). Biostatistical Analysis, fourth edition (New Jersey: Prentice-Hall Inc.).

Note Added in Proof

Since our paper was first submitted, one prediction of the model presented in the Discussion section has been verified independently by another team, and in view of the similarities in the conclusions based on very different methods and analysis, we have included this study in the reference list (Schummers et al., 2002).